Insights of Electrical Engineering and Technology
https://ojs.achpub.com/IEET

Research Article

A Circular-Patch-Loaded Spoof Surface Plasmon Polariton Leaky-Wave Antenna

Jingbo Shi[1,2], Wusheng Ji[1,2,*], Xinyi Li[1,2], and Haibo Li[1,2]

[1] Institute of Antenna and Microwave Techniques, Tianjin University of Technology and Education, Tianjin 300222, China
[2] School of Electronic Engineering, Tianjin University of Technology and Education, Tianjin 300222, China
E-mail: jiwusheng@tute.edu.cn

Received: 27 August 2025; **Revised:** 10 October 2025; **Accepted:** 21 October 2025

Abstract: To address the limitations of large size and narrow bandwidth in traditional leaky-wave antennas, we propose a frequency-scannable antenna based on a spoof surface plasmon polariton (SSPP) transmission line loaded with circular patches. The antenna comprises a coplanar waveguide (CPW), an SSPP transmission line, and circular patches. The coplanar waveguide excites the spoof surface plasmon polariton transmission line in even mode. Dual-beam scanning is achieved by introducing a phase difference through sinusoidal modulation of the unit cells and the integration of circular patches. Simulations show that the antenna operates from 4.5 to 8.7 GHz, corresponding to a relative impedance bandwidth of 65.1%. It achieves continuous backward-to-forward beam scanning over a 95° range. Owing to its simple structure, light weight, and wide scanning angle, the proposed antenna holds great promise for applications in UAVs, the Industrial Internet, and radar detection systems.

Keywords: leaky-wave antenna; spoof surface plasmon polariton; coplanar waveguide; beam scanning

1. Introduction

Leaky Wave Antennas (LWAs) represent a critical branch of traveling-wave antennas that radiate electromagnetic energy through precisely engineered surface wave leakage mechanisms [1]. Their operational principle relies on periodic modulations or customized waveguiding architectures that control the propagation characteristics of surface waves. This controlled perturbation enables partial energy leakage into free space, facilitating directional or scannable radiation patterns. In particular, planar LWs leverage their inherently planar geometry for straightforward fabrication using standard printed circuit board (PCB) processes. This affords significant advantages such as a low profile, ease of integration, structural simplicity, low cost, and convenient feeding schemes.

Spoof Surface Plasmon Polaritons (SSPPs) are electromagnetic waves supported by engineered subwavelength structures, which emulate the confinement and dispersion properties of optical Surface Plasmon Polaritons (SPPs) at lower frequencies [2]. Conventional SPPs, which are electromagnetic modes confined at metal-dielectric interfaces, are constrained by significant ohmic losses and stringent dimensional requirements (typically on the order of optical wavelengths). In contrast, SSPPs, realized through periodic artificial structures, overcome these limitations and exhibit remarkable slow-wave effects and broad operating bandwidths. These distinctive properties confer unique advantages for antenna design, including larger phase variation, more flexible dispersion control, and wider operational bandwidth. Consequently, SSPPs facilitate not only antenna miniaturization but also enhanced performance in areas such as high-gain radiation, wide-angle scanning, and broadband operation.

Copyright ©2025 Jingbo Shi, et al.
DOI: https://doi.org/10.37256/xxxx
This is an open-access article distributed under a CC BY license
(Creative Commons Attribution 4.0 International License)
https://creativecommons.org/licenses/by/4.0/

Ref. [2] pioneered a periodic structure featuring cubic grooves etched into 3D metal blocks to mimic conventional SPP properties at non-optical frequencies. The subsequent experimental verification of SSPP propagation at microwave frequencies was provided in Ref. [3]. A significant advancement was made in 2012 with the introduction of a conformal ultrathin SSPP structure, termed Conformal Surface Plasmons, which is compatible with fabrication on flexible printed circuit board (PCB) substrates [4].

The effective integration of SSPPs into microwave circuits necessitates tailored excitation and impedance-matching structures. Various designs have been developed for this purpose, including microstrip-to-SSPP transitions [5], CPW-to-SSPP adapters [6], coaxial-fed SSPP exciters [7], and tapered baluns [8]. These matching structures are crucial for enabling efficient modal conversion from conventional transmission line modes to confined SSPP modes. Complementing these experimental developments, Refs. [9, 10] conducted theoretical analyses of SSPP transmission line parameters, establishing a foundational equivalent lumped-circuit model for characterizing SSPP unit cells.

SSPP dispersion engineering enables wide-angle beam scanning in antennas by providing a frequency-dependent progressive phase shift across the aperture. Ref. [11] implemented a periodic modulation scheme, in which each unit cell acts as a leaky-wave radiator. The introduced discontinuities facilitate the conversion from slow-wave to fast-wave propagation, thereby enabling frequency-scanning operation. Ref. [12] engineered inter-element discontinuities into the SSPP waveguide geometry to deliberately perturb the mode, resulting in controlled radiation into free space. Ref. [13] utilized a sinusoidal modulation of the SSPP waveguide through periodic patterning, achieving a beam scanning range of 22.2°. Ref. [14] developed a beam-scanning antenna based on the odd-mode excitation of SSPPs, which enabled dual-endfire-beam scanning across a 90°angular sector. Although the aforementioned designs achieve frequency scanning, they are often hampered by excessively long modulation periods, resulting in bulky footprints. Moreover, they generally fail to support continuous beam scanning from the backward to the forward direction.

To overcome the limitations of insufficient scan range and excessive size, we designed a gradient SSPP metamaterial unit cell with sinusoidally modulated corrugations. The incorporation of circular patches on both sides of the transmission line introduces a progressive phase shift, facilitating the conversion from slow-wave to fast-wave propagation and ultimately enabling a wide scanning range from 135° to 270°. Furthermore, the antenna exhibits practical advantages such as low cost, structural simplicity, and favorable radiation patterns.

2. Antenna Structure and Technical Description

Figure 1 illustrates the architecture of the proposed SSPP frequency-scanning antenna, composed of a dielectric substrate, coplanar waveguide (CPW), and SSPP transmission line. A rectangular Rogers RO4350 material with relative permittivity of 3.66 and loss tangent of 0.004, with thickness h. Metallization on the top layer forms both CPW and SSPP transmission lines. The antenna architecture partitions into three functional part: Part I is CPW, Part II: gradient transition for impedance matching, Part III: core radiating zone with sinusoidal-profile corrugated center conductor. Detailed dimensional parameters are cataloged in Table 1.

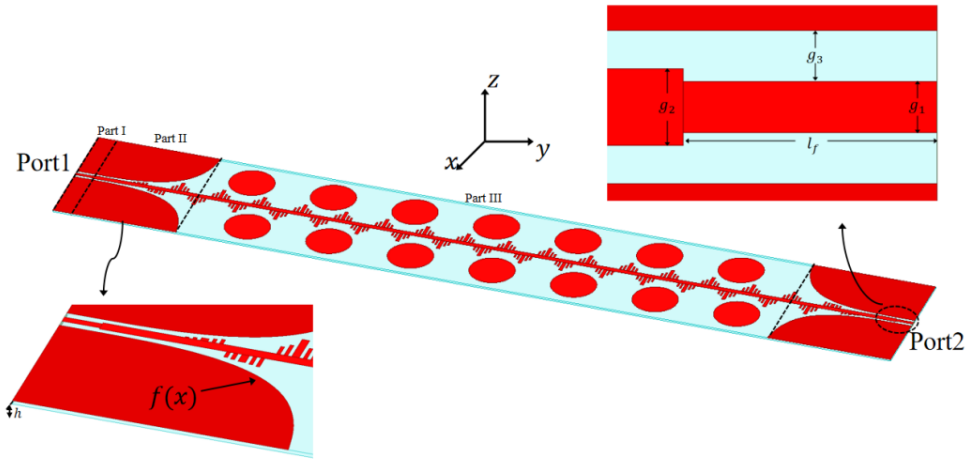

(a) Three-dimensional view of the antenna

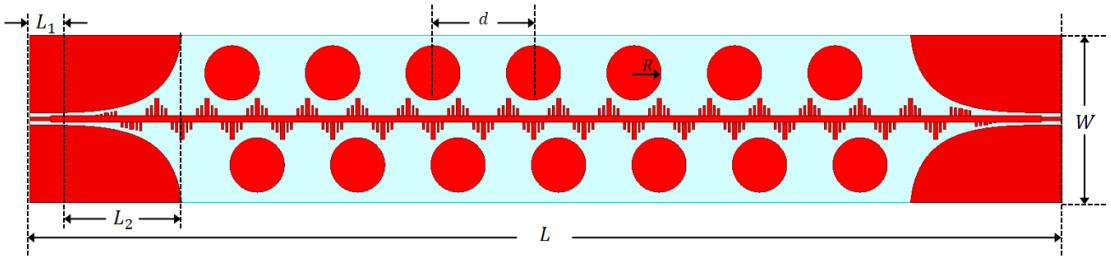

(b) Top view of the antenna

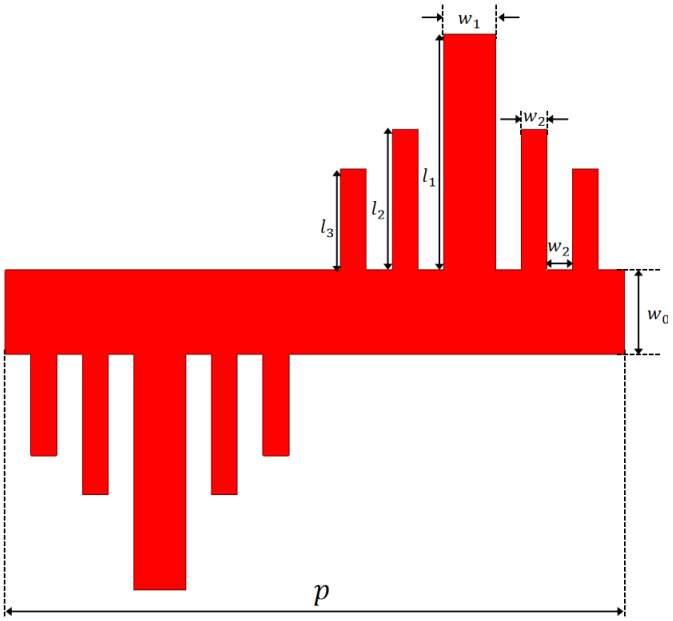

(c) Grid cell structure

Figure 1. Schematic diagram of the antenna structure

Table 1. Antenna Dimension Parameters

Parameters	L	L_1	L_2	l_1	l_2	l_3	l_f	p
Value (mm)	246.5	5	35	4.2	2.5	1.8	5	12
Parameters	W	w_0	w_1	w_2	h	g_1	g_2	g_3
Value (mm)	40	1.5	1	0.5	0.508	1	1.5	1

3. Antenna Design Process

Figure 2 illustrates the evolutionary design process of the proposed antenna, from the initial configuration (Antenna I) to the final optimized structure (Antenna III). The initial design, Antenna I, comprises an SSPP transmission line with uniform corrugations. Subsequent sinusoidal modulation of this transmission line results in Antenna II. Although this modification enhances the operational bandwidth, it does not yield significant frequency-scanning capability. The key optimization, incorporated in Antenna III, involves the integration of bilateral circular patches along the SSPP transmission line. Figure 3 compares the scattering parameters (S-parameters) of all three antenna configurations. The results verify effective even-mode transmission across the respective SSPP transmission lines.

To elucidate the operational mechanism, surface current distributions of Antenna III were simulated at distinct frequencies. Figure 4 presents the resultant current distributions: At 6.6 GHz, excitation from the right port confines EM waves along the SSPP transmission line, while bilateral circular patches enable energy coupling to the patches, facilitating efficient radiation into free space. S-parameters confirm even-

mode excitation throughout the SSPP transmission line, demonstrating effective transmission under even-mode drive, with a cutoff frequency near 8.7GHz. At 8.7GHz (post-cutoff), below cutoff, SSPP lines function as slow-wave transmission structures, but beyond cutoff, slow-wave modes become non-propagating, causing most EM energy to reflect back to the port. Furthermore, it can be clearly observed that the energy is primarily concentrated on the longest stub within the unit cell; therefore, the length of this longest stub is the most critical parameter for the antenna.

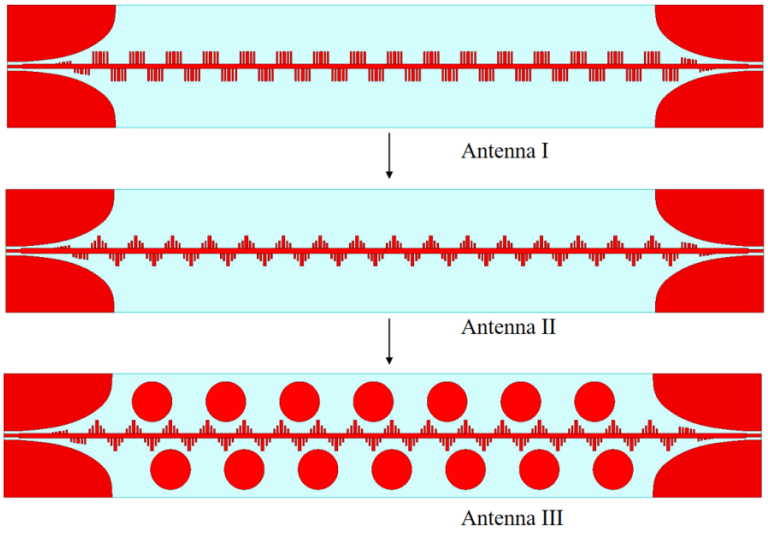

Figure 2. Evolution of antenna design plot

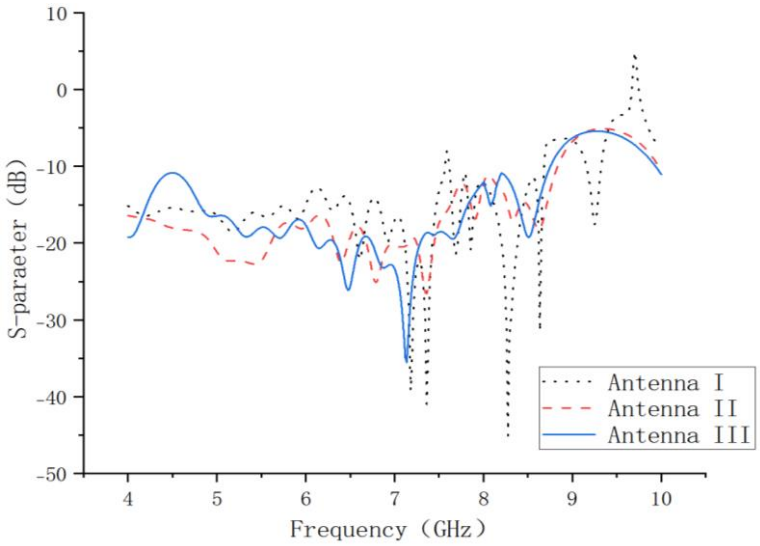

Figure 3. Comparison of S11 for Three Antennas

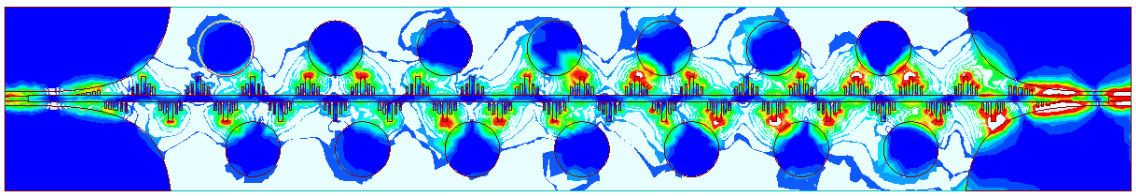

(a) 6.6GHz Current distribution

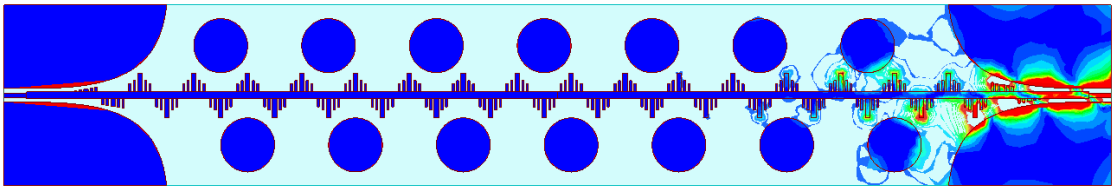

(b) 8.75GHz Current distribution

Figure 4. Current distribution on antenna surface plot

4. Working Principle of The Proposed Antenna

Figure 5 shows the equivalent circuit of the transmission line unit cell structure. At impedance discontinuities, the structure is modeled as a series reactance (either inductive or capacitive) flanked by two length-corrected transmission line segments. Similarly, right-angle bends are represented by a shunt capacitance connected to two short transmission line sections. Furthermore, each individual metal patch contributes a capacitance due to the fringing electric fields that terminate at infinity.

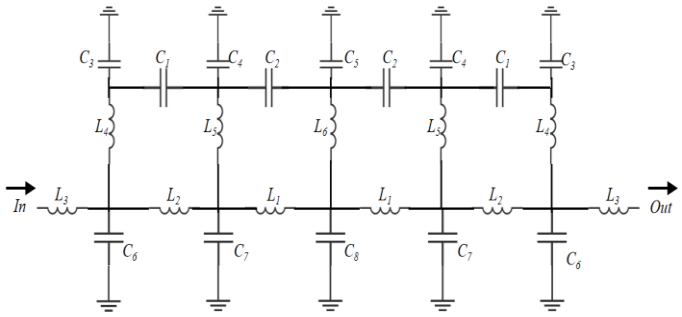

Figure 5. Equivalent circuit diagram of unit structure

The antenna was simulated using HFSS software, demonstrating excellent performance in the 4.5GHz~8.7GHz frequency band. The following analysis focuses on optimizing S11 parameters and investigating the impact of unit structure length on S parameters. Figure 6 illustrates the variation in S11 characteristics when adjusting the length l_1 of the central grid in the unit structure. It is evident that l_1 significantly affects the antenna's impedance bandwidth. During electromagnetic wave propagation, energy primarily concentrates at the grid structure. Because the energy of electromagnetic waves is mainly concentrated at the fence during propagation, the sinusoidal modulated SSPP unit structure has a strong binding effect on electromagnetic waves, which can make electromagnetic waves transmit along the direction of transmission lines.

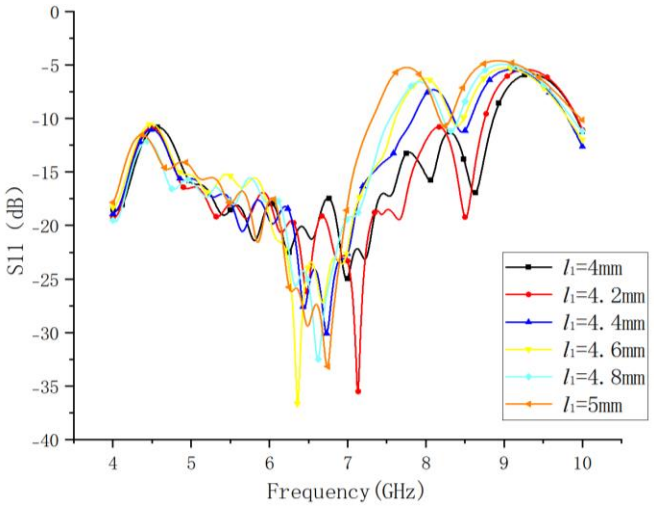

Figure 6. S11 varies with the parameter l_1

The dispersion curve of slow-wave dominant modes with varying groove depths, obtained using an intrinsic mode solver, is shown in Figure 7(a). The dispersion curve of the unit cell structure deviates significantly from that of light rays, indicating its wave vector exceeds that of free-space light waves. The dominant modes remain entirely within the non-radiative slow-wave region, and as groove depth increases, the slope of the dispersion curve gradually becomes steeper while the cutoff frequency progressively decreases. Since SSPPs transmission lines support surface slow-wave modes $k_{sspp}>k_0$, k_{sspp} represents the wave vector of SSPPs, their surface waves are non-radiative. To achieve radiation, we employ perturbation methods to excite higher harmonics. According to Floquet's theorem, the phase constant satisfies the equations:

$$\beta_n = \beta_0 + \frac{2\pi n}{p} \quad n = 0, \pm 1, \pm 2 \ldots \tag{1}$$

where β_0 denotes the phase constant of the fundamental harmonic. Only single harmonics meeting periodic radiation conditions can generate leakage radiation, so we typically use spatial harmonics with n = −1 Due to their positive and negative properties, the radiated beam can propagate forward or backward, with the radiation direction θ represented by β_{-1} as:

$$\theta = \arcsin\frac{\beta_{-1}}{k_0} \tag{2}$$

The dispersion characteristic curve of the −1st harmonic after modulation can be obtained by translating the fundamental mode dispersion curve along the negative horizontal axis by 180°, as shown in Figure 7(b).

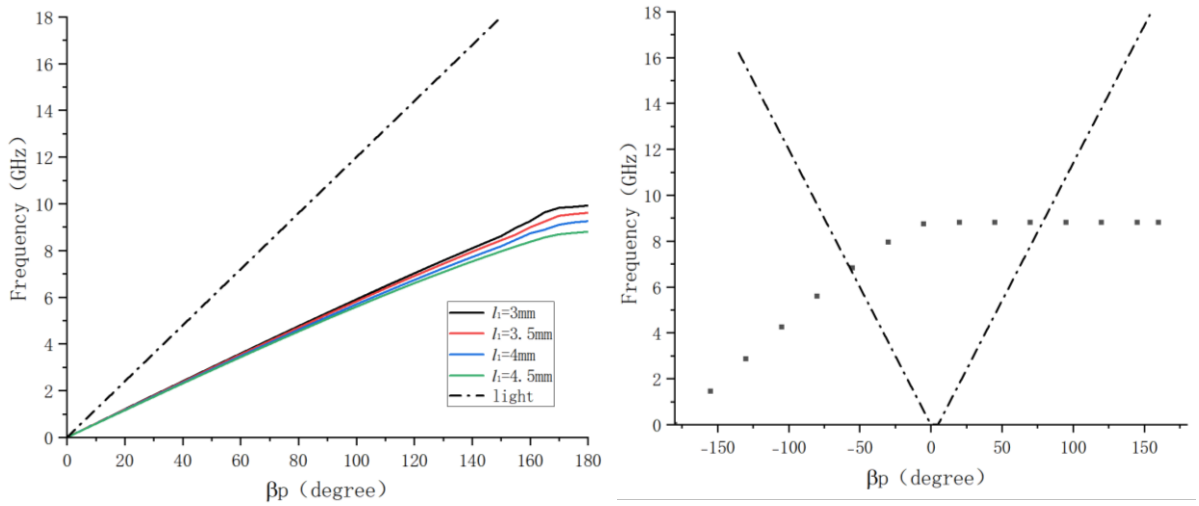

(a) The variation of the cutoff frequency with the parameter l_1

(b) −1 harmonic dispersion characteristic curve

Figure 7. Introduction of discontinuity in the dispersion characteristic curve of unit structure

Figure 8 shows the l_2 and l_3 have little influence on the impedance bandwidth of the antenna. When the SSPPs transmission line works, the energy is mainly concentrated at the longest branch of the unit structure fence, so the change of l_2 and l_3 has little influence on the impedance bandwidth of the antenna.

Secondly, considering that during the operation of the SSPPs transmission line, energy couples to the circular patches, the radius of the circular patches has a certain influence on the S11 parameter. As shown in Figure 9(a), the S11 parameter changes significantly with the variation in the circular patch radius, because the circular patches also couple energy and radiate it into free space, leading to this significant change in S11.

The SSPP unit cell structure can be considered a slow-wave transmission line, which radiates energy directly into free space by itself. The transmission line and the circular radiating patches are excited to generate radiation. During propagation, electromagnetic waves undergo continuous leakage radiation from the waveguiding structure itself into free space. The current distribution across the circular patches of the SSPP transmission line unit cell at the central frequency (6.6 GHz) is presented in Figure 9(b). Analysis

reveals that the currents in two adjacent unit cells are in phase opposition, indicating that the electromagnetic energy is highly localized and confined within the corrugated region, effectively preventing energy leakage.

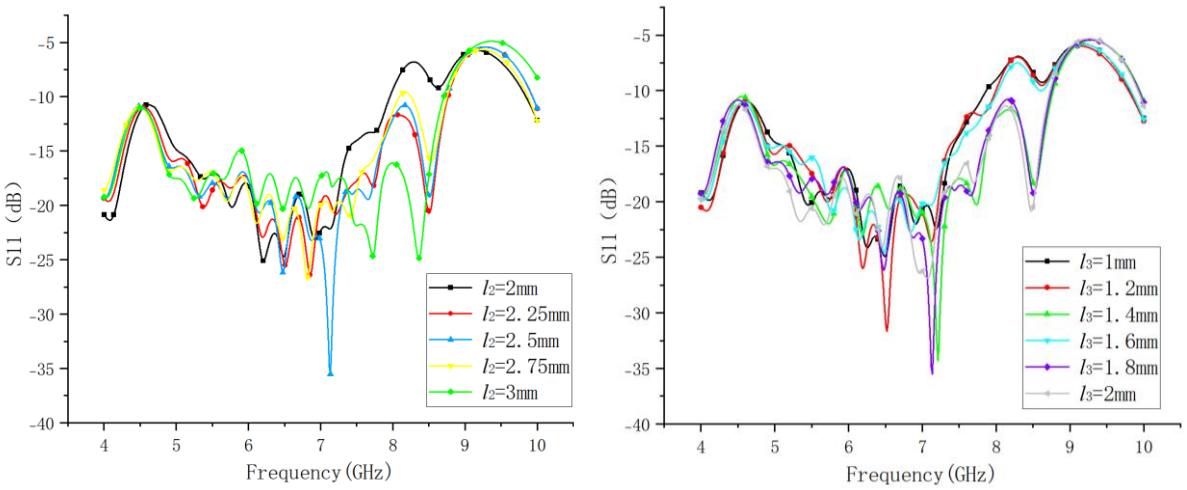

(a) The variation of S11 with parameter l_2 (b) The variation of S11 with parameter l_3

Figure 8. The variation of S11 with parameters l_2 and l_3

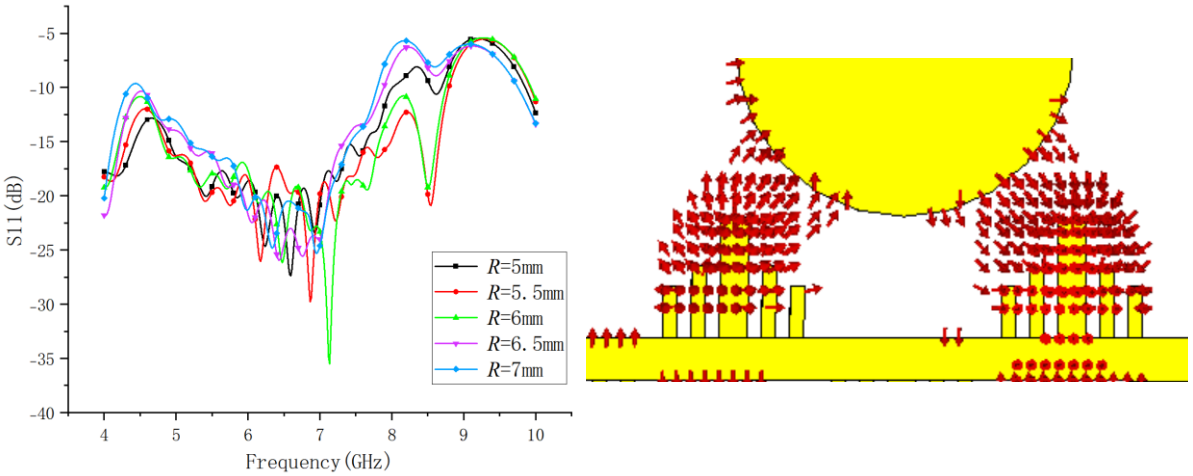

(a) The variation of S11 with parameter R (b) Current distribution diagrams of the unit cell and circular patches

Figure 9. Influence of circular patch on antenna parameters

5. Antenna Simulation Results

Figure 10 presents the simulated reflection coefficient (S11) of the proposed antenna design. A comprehensive performance evaluation was conducted using two independent full-wave electromagnetic simulators, HFSS and CST, for cross-verification. The HFSS simulations indicate an operational bandwidth from 4.5 to 8.7 GHz, while CST results show a range from 4.4 to 8.60 GHz. Moreover, the profiles of both S11 and S21 parameters obtained from the two simulators show excellent agreement. In summary, the strong agreement between the HFSS and CST simulation results mutually validates the design and confirms the reliability of the antenna's performance.

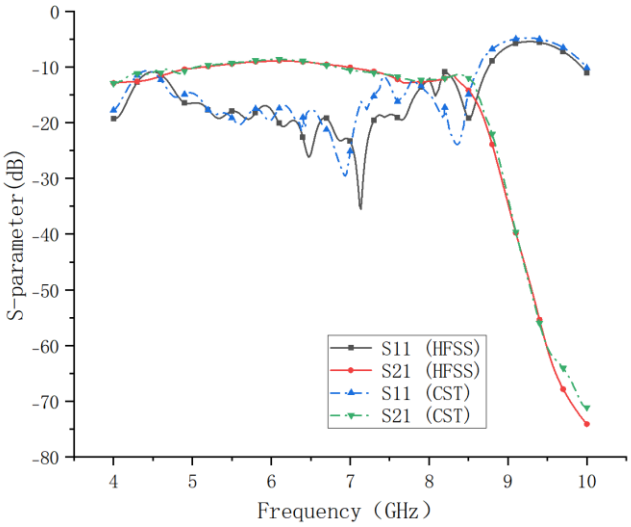

Figure 10. Simulation results of S-parameters for HFSS and CST

Figure 11 shows the radiation patterns of the antenna. When operating at 4.90 GHz, 5.72 GHz, 6.41 GHz, 7.10 GHz, 7.66 GHz, and 8.02 GHz, the antenna's maximum radiation beam directions are 270°, 230°, 210°, 195°, 180°, and 175°, respectively. Thus, the main beam of the proposed SSPPs LWA can scan from 270° to 175°. Furthermore, as the frequency increases, the antenna gain also increases. This leads to a narrowing of the antenna's radiation beam. Since the antenna is excited in the even mode, it operates as a dual-beam leaky-wave antenna.

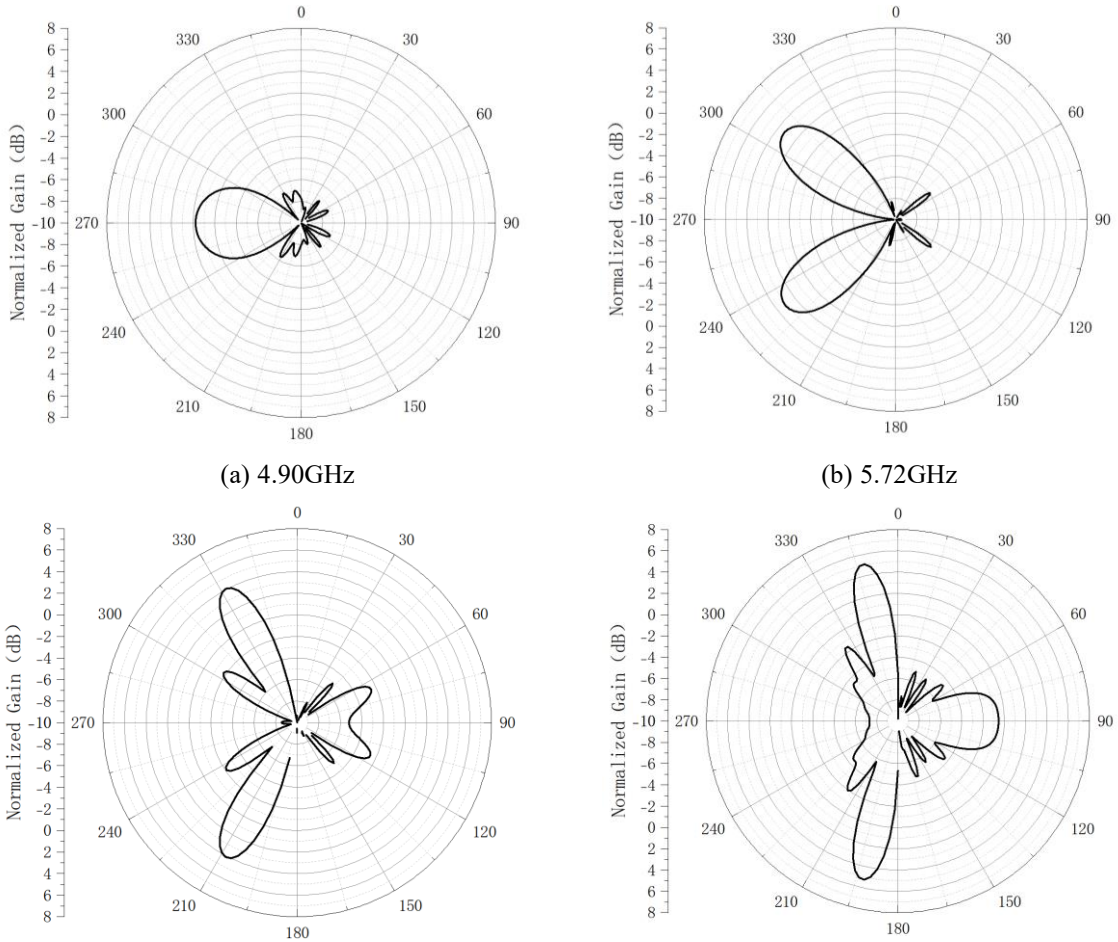

(a) 4.90GHz (b) 5.72GHz

(c) 6.41GHz (d) 7.10GHz

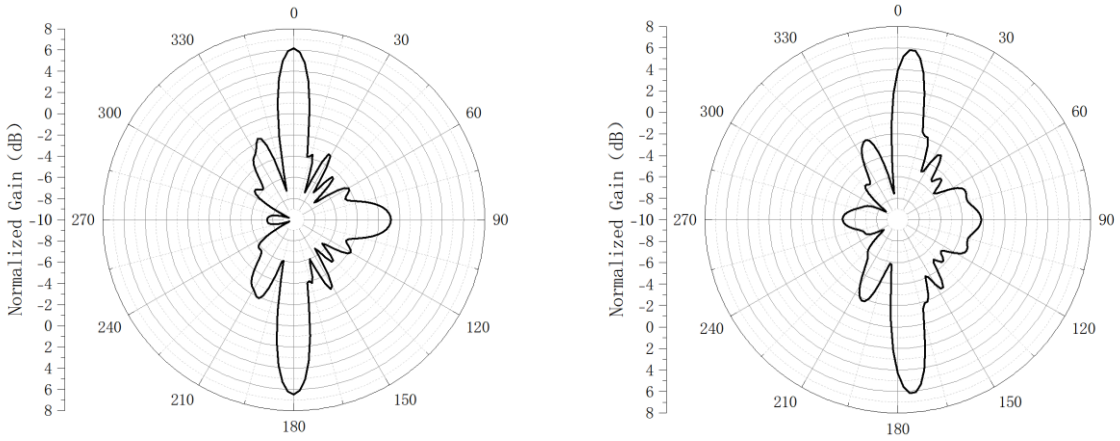

(e) 7.66GHz (f) 8.02GHz

Figure 11. Antenna radiation pattern

As illustrated in Figure 12(a), the measured S-parameters of the fabricated antenna confirm an operational bandwidth spanning from 4.5 to 8.7 GHz, which corresponds to a relative impedance bandwidth of 65.1%. The corresponding radiation patterns, presented in Figure 12(b), demonstrate continuous main beam scanning from −90° to 5°, achieving a total frequency-scanning range of 95° from the backward to the forward direction.

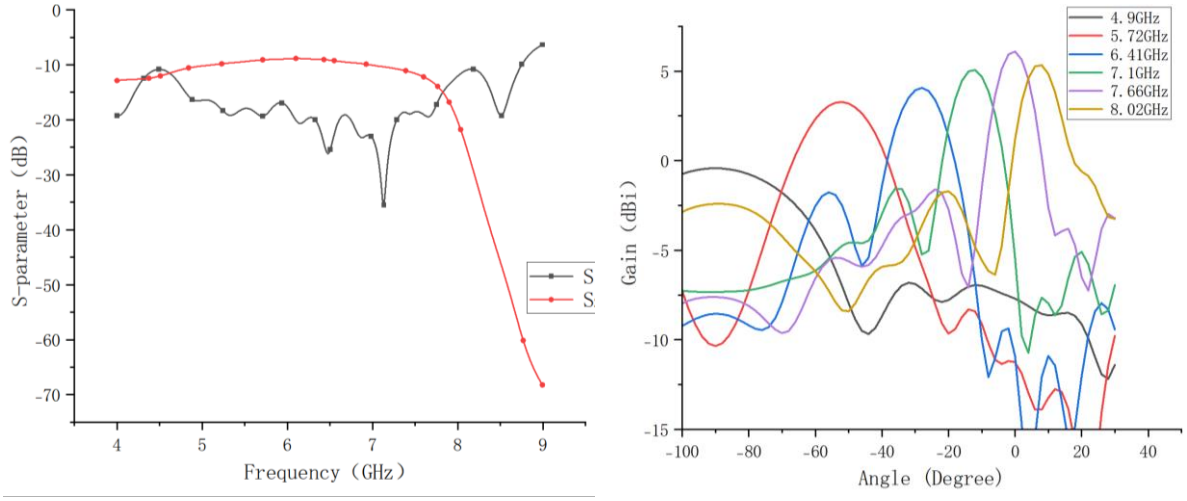

(a) The S-parameters of the antenna (b) Radiation Patterns of the Antenna Across Various Frequencies

Figure 12. S-parameter sand direction diagram of the antenna

A performance comparison between the proposed antenna and other recently reported SSPP-based LWAs is summarized in Table 2. The data demonstrates that our design achieves a competitive balance of a wide impedance bandwidth and an extensive beam-scanning range. Furthermore, it attains these performance metrics with a notably compact form factor.

Table 2. The Antenna Proposed is Compared to Other Antennas

Ref.	Size (mm)	Imp. BW (GHz)	Imp. BW (%)	Beam-Scanning Range (°)	Maximum Gain (dBi)
[15]	32×221	8.65~9.5	9.3	−65°~+2°	8.2
[16]	-	4.2~5.5	26.8	−30°~+30°	-
[17]	22×229.5	9.7~13.3	31.3	-46°~+22°	13.4
[18]	-	22.5~35	26	+5°~+76°	13
This work	40×246.5	4.5~8.7	65.1	−90°~+5°	6.3

6. Conclusion

This paper presents a leaky-wave antenna (LWA) based on a modulated spoof surface plasmon polariton (SSPP) transmission line. To facilitate the conversion from slow surface waves to fast radiating waves, circular patches are symmetrically integrated along both sides of the SSPP transmission line, dual-beam scanning is achieved by introducing a phase difference through sinusoidal modulation of the unit cells and the integration of circular patches. The proposed SSPP-LWA achieves a 65.1% impedance bandwidth (4.5–8.7 GHz) and a wide-angle beam-scanning range of 95°, covering from −90° to +5°. Although the maximum gain is relatively modest, the antenna offers compelling advantages, including a wide bandwidth, planar and low-profile architecture, and a large scanning angle, endowing it with broad application potential in satellite communication and radar systems.

Author Contributions

Simulation, computation and writing, J.S.; Review and revision, W.J.; Technical support, X.L. and H.L.

Funding

This work is supported by Tianjin Key Projects of Research and Development and Science and Technology Support in 2020 (20YFZCGX00700), and Tianjin Enterprise Science and Technology Commissioner Project in 2022 (22YDTPJC00330).

Acknowledgments

The authors express their reciprocal appreciations for efficient collaborations.

Conflict of Interest

There is no conflict of interest for this study.

References

[1] K. C. Gupta, "Characteristics of leaky wave antennas-A review," *IEICE Proceedings Series*, vol. 4, no. 3A4-3, 1978.

[2] J. B. Pendry, L. Martin-Moreno, and F. J. Garcia-Vidal, "Mimicking surface plasmons with structured surfaces," *Science*, vol. 305, no. 5685, pp. 847-848, 2004. DOI: 10.1126/science.1098999

[3] A. P. Hibbins, B. R. Evans, and J. R. Sambles, "Experimental verification of designer surface plasmons," *Science*, vol. 308, no. 5722, pp. 670-672, 2005. DOI: 10.1126/science.1109043

[4] X. Shen, T. J. Cui, D. Martin-Cano, et al., "Conformal surface plasmons propagating on ultrathin and flexible films," *Proceedings of the National Academy of Sciences*, vol. 110, no. 1, pp. 40-45, 2013. DOI: 10.1073/pnas.1210417110

[5] Z. Liao, J. Zhao, B. C. Pan, et al., "Broadband transition between microstrip line and conformal surface plasmon waveguide," *Journal of Physics D: Applied Physics*, vol. 47, no. 31, p. 315103, 2014. DOI: 10.1088/0022-3727/47/31/315103

[6] H. F. Ma, X. Shen, Q. Cheng, et al., "Broadband and high-efficiency conversion from guided waves to spoof surface plasmon polaritons," *Laser & Photonics Reviews*, vol. 8, no. 1, pp. 146-151, 2014. DOI: 10.1002/lpor.201300118

[7] D. Tian, R. Xu, G. Peng, et al., "Low-profile high-efficiency bidirectional endfire antenna based on spoof surface plasmon polaritons," *IEEE Antennas and Wireless Propagation Letters*, vol. 17, no. 5, pp. 837-840, 2018. DOI: 10.1109/LAWP.2018.2818109

[8] A. Kianinejad, Z. N. Chen, and C. W. Qiu, "Design and modeling of spoof surface plasmon modes-based microwave slow-wave transmission line," *IEEE Transactions on Microwave Theory and Techniques*, vol. 63, no. 6, pp. 1817-1825, 2015. DOI: 10.1109/TMTT.2015.2422694

[9] A. Kianinejad, Z. N. Chen, and C. W. Qiu, "Full modeling, loss reduction, and mutual coupling control of spoof surface plasmon-based meander slow wave transmission lines," *IEEE Transactions on Microwave Theory and Techniques*, vol. 66, no. 8, pp. 3764-3772, 2018. DOI: 10.1109/TMTT.2018.2841857

[10] T. Wang, L. Liu, H. Ni, et al., "A full-angle scanning leaky wave antenna based on odd-mode SSPP from backfire to endfire," *IEEE Transactions on Antennas and Propagation*, vol. 71, no. 11, pp. 8570-8579, 2023. DOI: 10.1109/TAP.2023.3311612

[11] J. J. Xu, X. Jiang, H. C. Zhang, et al., "Diffraction radiation based on an anti-symmetry structure of spoof surface-plasmon waveguide," *Applied Physics Letters*, vol. 110, no. 2, 2017.

[12] J. J. Xu, H. C. Zhang, Q. Zhang, et al., "Efficient conversion of surface-plasmon-like modes to spatial radiated modes," *Applied Physics Letters*, vol. 106, no. 2, 2015. DOI: 10.1063/1.4905580

[13] G. S. Kong, H. F. Ma, B. G. Cai, et al., "Continuous leaky-wave scanning using periodically modulated spoof plasmonic waveguide," *Scientific Reports*, vol. 6, no. 1, p. 29600, 2016. DOI: 10.1038/srep29600

[14] X. Du, J. Ren, H. Li, et al., "Design of a leaky-wave antenna featuring beam scanning from backfire utilizing odd-mode spoof surface plasmon polaritons," *IEEE Transactions on Antennas and Propagation*, vol. 69, no. 10, pp. 6971-6976, 2021. DOI: 10.1109/TAP.2021.3076166

[15] Z.Peng, W. Yang, S. Shi, et al., "High scanning rate asymmetrical dual-beam leaky wave antenna using sinusoidally modulated reactance superposing surface," *IEEE Transactions on Antennas and Propagation*, vol. 70, no. 12, pp. 12258-12263, 2022. DOI: 10.1109/TAP.2022.3209181

[16] B. Zhang, Z. Li, and J. Wang, "Conformal Leaky-Wave Antenna with Scanning Beam Based on Spoof Surface Plasmon Polaritons," in *2024 IEEE 10th International Symposium on Microwave, Antenna, Propagation and EMC Technologies for Wireless Communications (MAPE)*, 2024, pp. 1-3. DOI: 10.1109/MAPE62875.2024.10813684

[17] Q. Ma and L. Liu, "A High-gain Leaky Wave Antenna with Open-Stopband Suppression Based on SSPPs," in *2024 IEEE MTT-S International Microwave Workshop Series on Advanced Materials and Processes for RF and THz Applications (IMWS-AMP)*, 2024, pp. 1-3. DOI: 10.1109/IMWS-AMP62793.2024.10966779

[18] W. Fu, D. Shen, H. Huang, et al., "Wide-angle scanning gain stable millimeter wave leaky wave antenna based on ISGW," in 2023 International Applied Computational Electromagnetics Society Symposium (ACES-China), 2023, pp. 1-2. DOI: 10.23919/ACES-China60289.2023.10249700